Probing the Spin Dimensionality in Single-Layer CrSBr Van Der Waals Heterostructures by Magneto-Transport Measurements

Carla Boix-Constant, Samuel Mañas-Valero, Alberto M Ruiz, Andrey Rybakov, Krzysztof Aleksander Konieczny, Sébastien sebastien Pillet, José J Baldoví, Eugenio Coronado

Probing the spin dimensionality in single-layer CrSBr van der Waals heterostructures by magneto-transport measurements

Carla Boix-Constant,[a] Samuel Mañas-Valero,[a] Alberto M. Ruiz,[a] Andrey Rybakov,[a] Krzysztof Aleksander Konieczny,[b] Sébastien Pillet,[b] José J. Baldoví,[a] Eugenio Coronado.[a*]*

[a] Instituto de Ciencia Molecular (ICMol), Universitat de València, Catedrático José Beltrán 2, Paterna 46980, Spain.

[b] Université de Lorraine, CNRS, CRM2, 54500 Nancy, France.

e-mail: samuel.manas@uv.es, eugenio.coronado@uv.es

KEYWORDS: 2D materials, 2D magnets, van der Waals heterostructures, quantum materials, electrical properties, DFT calculations

Two-dimensional (2D) magnetic materials offer unprecedented opportunities both in terms of fundamental concepts and applied devices with special relevance in the fields of spintronics and magnonics.[1] Beyond the pioneering studies on CrI_3 and $Cr_2Ge_2Te_6$,[2,3] the family of 2D magnets has expanded to layered antiferromagnets with different spin anisotropies[4–6] and spin textures.[7] However, all these compounds are highly insulating, thus limiting their possibilities for being integrated into devices. Of particular interest is the case of the layered metamagnet CrSBr, a 2D semiconductor formed by ferromagnetic layers (T_c ~ 150 K) coupled antiferromagnetically between them. This material exhibits a rich physical scenario, including thermal spin dimensionality crossovers and low-temperature hidden order (T* ~ 40 K).[8–11] Here, we inspect the magneto-transport properties of monolayer, bilayer and trilayer CrSBr integrated into vertical van der Waals heterostructures. Our results in the monolayer limit demonstrate (1) the marked low dimensional character of the ferromagnetic layer, with short-range correlations extending at temperatures well above T_c, (2) a spin anisotropy, with the spins spontaneously aligned along the easy axis (*b*) of the plane, (3) a reorientation of these spins along *a* and *c* upon applying a moderate magnetic field in these directions, and (4) the appearance of field-induced phases in these two directions below *ca.* 30-40 K due to a cooperative freezing of the spins. In the multilayer case, a spin valve-like behavior is also observed characterized by a negative MR strongly enhanced below T*. Overall, the present results, supported by first-principles calculations, show that the monolayer and bilayer of CrSBr capture most of the physics present in the bulk, offering new insights into the physics of 2D magnets and the integration of these layers into vertical spintronic devices.

A single layer of CrSBr is formed by the following sextuple arrangement of atoms along the *c* axis: bromine/chromium/sulfur/sulfur/chromium/bromine (**Figure 1.a-b**). Every chromium atom is hexacoordinated and is linked to the nearest chromium neighbor through sulfur and bromine atoms along the *a* axis (forming 95º and 89º, respectively) and just by sulfur along the *b* (160º) and *c* axis (97º). Thus, the crystal structure of CrSBr can be described as layers of CrS_4Br_2 distorted octahedra, sharing S-Br edges along the *a* axis, S corners along the *b* axis, and S-S edges along the diagonal of the *ab* plane, forming a rectangular 2D magnetic lattice.[12] Although CrSBr was first described in 1990's by Beck[13] and their magnetic properties were soon described by Göser *et al.*,[14] this layered material has gained a recent attention due to its magnetic, optical and electronic properties in the 2D limit.[15–17] The single layer orders ferromagnetically (T_c ~ 150 K), as observed by second harmonic generation.[18] However, in bulk, the layers couple between them antiferromagnetically undergoing a long-range order at T_N ~ 140 K –A type antiferromagnetism– and behave as a metamagnet, being possible to switch the magnetization of the layers from antiparallel to parallel configurations with an external magnetic field ($B_{sat,\ a\ axis}$ ~ 1.0 T, $B_{sat,\ b\ axis}$ ~ 0.6 T and $B_{sat,\ c\ axis}$ ~ 2.0 T at 2 K, where B_{sat} states for the saturation field at 3 Bohr magnetons, as expected for a chromium system with S = 3/2; **Figure 1.d**).[9–11]

Regarding magneto-transport experiments, Telford *et al.* observed large negative magnetoresistance (MR) in bulk due to the layered antiferromagnetism exhibited by CrSBr.[11] When the system is thinned-down to the monolayer, this negative MR is maintained up to the bilayer case but turns to be positive in the monolayer when the field is applied along the *a* and *c* direction, remaining zero along *b*.[8] However, this scenario is more intriguing since, recently, Wu *et al.* have reported on the existence of both positive and negative MR in a CrSBr thin-layer depending on the current direction (parallel to the *a* or *b* crystallographic axis), being the system

better described as a quasi-1D semiconductor.[19] In all these cases, a striking enhancement of the MR below T* ~ 30-40 K, quoted as a *hidden order,* has been observed. Telford *et al.* ascribed this enhanced MR to the ferromagnetic ordering of magnetic defects[8] although Wu *et al.* consider its origin in terms of incoherently coupled 1D electronic chains.[19] In this line, López-Paz *et al.* have studied bulk CrSBr by a battery of magnetic techniques, associating the hidden order to a spin-dimensionality crossover caused by a slowing down of the magnetic fluctuations below T_S ~ 100 K and an eventually spin freezing at T*.[10] In addition, CrSBr multi-layers have been shown to be good candidates to induce spin-polarization in graphene-based van der Waals heterostructures.[20,21] Thus, CrSBr atomically-thin layers are an attractive low-dimensional magnetic system with fundamental open questions and appealing potential in spintronic and magnonic applications.

In this work, we inspect the magneto-transport properties of mono-, bi- and tri-layer CrSBr with the current passing along the *c* direction by fabricating vertical van der Waals heterostructures with few-layers graphene and atomically-thin metals as 2H-$NbSe_2$ or 2H-TaS_2.

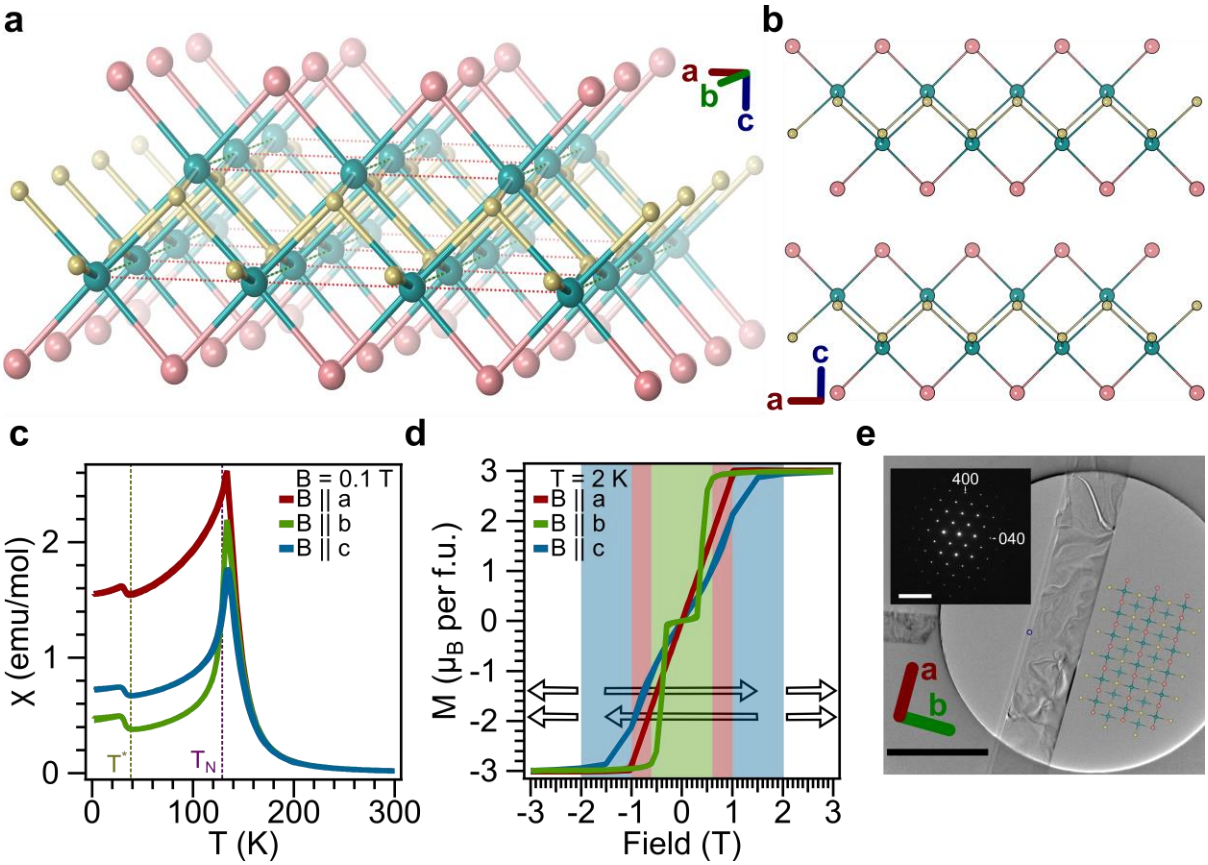

Figure 1.- Structural and magnetic properties of bulk CrSBr. a) Structure of a single layer of CrSBr, where the chromium, sulfur and bromine atoms are represented as cyan, yellow and pink balls. b) Stacking of CrSBr layers along the *c* axis. c) Magnetic susceptibility of bulk CrSBr under an applied magnetic field of 0.1 T. Reported antiferromagnetic (T_N) and low-temperature hidden-order phase (T*) temperatures are marked as pink and yellowish vertical dashed lines. d) Magnetization of CrSBr at 2 K. Saturation of the magnetization at 3 Bohr magnetons, corresponding to S = 3/2, is obtained when the layers are coupled ferromagnetically (represented as inset arrows). e) Transmission electron microscopy image of a CrSBr exfoliated flake together with an oriented structure cartoon of CrSBr. Scale bar: 2 μm. Inset: selected area diffraction pattern measured at the area enclosed in a blue circle. Scale bar: 10 nm^{-1}.

High-quality CrSBr crystals are grown by solid state techniques (see **Methods**). The structure is solved by single crystal X-Ray diffraction at different temperatures, being the results in agreement with those reported by Telford *et al.*[11] CrSBr crystallizes in the structure type FeOCl,[11,13,14] which is adopted by the isostructural compounds MOX (M = Ti, V, Cr, Fe ; X = Cl, Br), in the orthorhombic space group Pmmn with two formula units per unit cell.[22–25] The whole family of MOX compounds exhibit magnetic transitions, which are accompanied by lattice and structural distortions owing to magnetoelastic coupling, evidenced by single crystal or powder X-

ray diffraction. In TiOCl and TiOBr, a spin-Peierls transition inducing a lowering of symmetry from orthorhombic to monoclinic has been detected by the development of twofold superstructure reflections below T_c, indicating a dimerization of the Ti chain.[24] The lowering of the point symmetry was revealed by a splitting of reflections. A similar monoclinic distortion has also been characterized for CrOCl,[25] VOCl[23] and FeOCl.[22]

In order to correlate the electronic and magnetic behavior of CrSBr and its magneto-electric anisotropy to a possible underlying structural phase transition, the crystal structure and infrared spectra has been monitored as a function of temperature below 75K using single crystal X-ray diffraction (**Supplementary Section 1.2**). Contrary to TiOCl, no superstructure reflections were detected in the reconstruction of the reciprocal lattice, ruling out any phase transition of the spin-Peierls type. Complete crystal structures have been determined and refined at T = 10 K and T = 75 K. No symmetry change, and especially no symmetry lowering to monoclinic is observed contrary to the monoclinic distortions characterized for the MOX compounds. The corresponding structures can be described both in the Pmmn space group. The distortion of the CrS_4Br_2 octahedra is preserved while lowering the temperature. This structural analysis is in agreement with the structures reported at 15 K and 50 K by Telford *et al.*[11] and the powder X-ray crystallography results of Lopez-Paz *et al.*[10] The reciprocal space was reconstructed at all temperatures, in order to detect a subtle monoclinic distortion. Still, no splitting of the Bragg reflections was evidenced (**Supplementary Section 1.2**). The infrared spectrum of CrSBr was as well monitored as a function of temperature. The vibrational absorption bands at 265 cm^{-1} and 322 cm^{-1} do not experience any significant shift, intensity change or splitting upon temperature lowering from 90K to 10K (**Supplementary Section 1.3**). This result further strengthens the idea that no structural phase transition occurs in that temperature range.

Once a structural transition has been discarded in bulk CrSBr, we inspect the magnetic properties of mono-, bi- and tri-layer CrSBr by incorporating them in vertical van der Waals heterostructures (**Figure 2**) based on few-layers graphene and atomically-thin metals as 2H-$NbSe_2$ or 2H-TaS_2. 2D layers are obtained by mechanical exfoliation from their bulk counterparts (see **Methods**) and deposited onto 285 nm SiO_2/Si substrates under strict inert conditions since CrSBr atomically-thin layers degrade in air.[8] The CrSBr thin-layers are inspected by optical microscopy and identified by their optical contrast. The maximum optical contrast for a CrSBr monolayers is observed upon 550 nm illumination (see **Supplementary Section 2** for further details). Typical CrSBr flakes exhibit a ribbon shape, being the long (short) direction associated with the *a* (*b*) axis, as verified by optical contrast, Raman spectroscopy and selected area electron diffraction patterns obtained by transmission electron microscopy (**Figure 1.e** and **Supplementary Section 1.4** and **Supplementary Section 2**). The van der Waals heterostructures are fabricated by assembling the different layers and depositing them on top of a pre-patterned electrical contacts (see **Methods**), as shown in **Figure 2.a**. Importantly, the heterostructure is encapsulated between hexagonal boron-nitride thin-layers for avoiding any possible degradation.

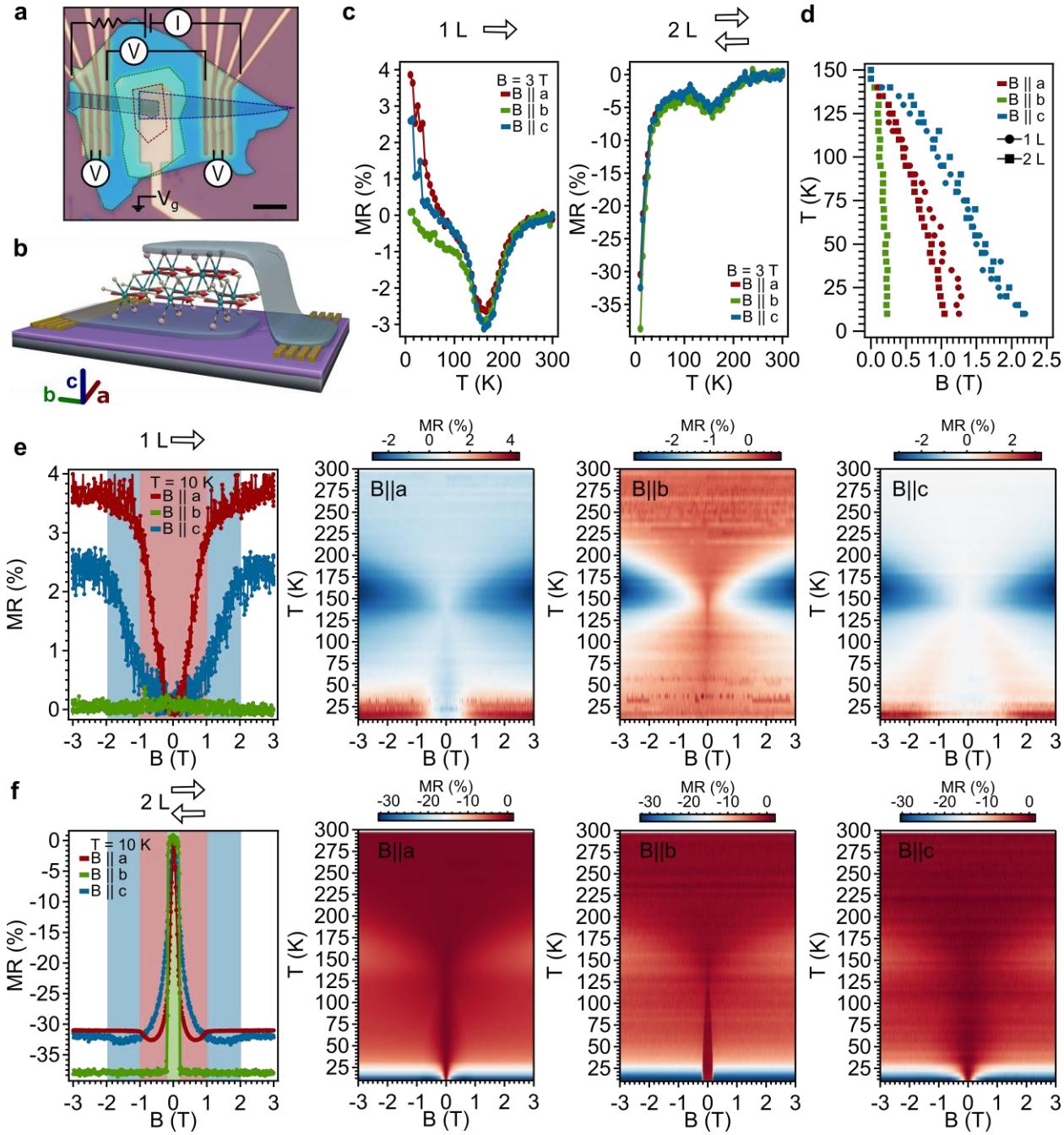

Figure 2.- Magneto-transport properties of monolayer and bilayer CrSBr vertical van der Waals heterostructures. a) Typical van der Waals heterostructure device. Top and bottom few-layers graphene are enclosed within blue dash lines and the CrSBr with red dashed line. The whole heterostructure is encapsulated between h-BN, marked with green dashed lines. Scale bar: 5 µm. b) Artistic view (not to scale) of the vertical van der Waals heterostructure. The few-layers graphene is represented in grey and the CrSBr structure is shown in a ball-and-stick representation (chromium, sulfur and bromine atoms are represented in cyan, yellow and pink colours, respectively). c) Temperature dependence of the magneto-resistance (MR) for a monolayer and bilayer CrSBr van der Waals heterostructure based on few-layers $NbSe_2$ (devices A.5 and B.6 in the **Supplementary Information Section 3**, respectively) for fields (3 T) applied along the different crystallographic orientations. d) Diagram for the temperature *vs.* magnetic fields values where a switching is observed in panels e and f. e-f) Field dependence of the magneto-resistance (MR) at 10 K for a monolayer (device A.5) and bilayer (device B.6) CrSBr van der Waals heterostructure based on few-layers $NbSe_2$ for fields applied along the different crystallographic orientations (first panel) together with the temperature and field dependence of the magneto-resistance when the magnetic field is applied along the *a* axis (second panel), the *b* axis (third panel) and the *c* axis (fourth panel). Magneto-resistance (MR) is defined as MR (%) = 100·[R(B) – R(0)]/R(0).

All our van der Waals heterostructure devices (13 devices in total) exhibit ohmic behavior from room to low temperatures (**Supplementary Section 3.4)**, in contrast to the sigmoidal IV curves reported for horizontal CrSBr devices.[19] In **Figure 2.c**, we compare the temperature dependence of the MR for a monolayer and bilayer CrSBr van der Waals heterostructure. The two cases exhibit almost zero MR –defined as MR = 100[R(B) – R(0)]/R(0), where B is the external magnetic field– in the paramagnetic phase for temperatures above T ~ 240 K. Below this temperature, the MR turns negative and decreases until T_c ~ 150 K is reached, when it reverts the tendency and enhances down to T ~ 100 K. At lower temperatures, the monolayer and the bilayer exhibit different trends. In the monolayer case, the MR continue its steady increase with a more pronounced increase below T*, being positive for fields applied along the *a* and *c* axis and almost zero for fields along the *b* axis. In contrast, for the bilayer case, the MR remains negative and with a weak temperature variation down to T*, when it decreases considerably. This behavior does not exhibit significant differences among devices (see **Supplementary Section 3**) and is comparable with previous measurements in horizontal devices.[8] Nonetheless, raw resistance curves are considerably different to the ones reported for atomically-thin layers measured in this horizontal geometry (see comparative in **Supplementary Section 3.2**). Thus, in the horizontal devices there is a decrease in conductance in the 300 K - 200 K range followed by a metallic regime until *ca.* 130 K and a final crossover to a semiconducting/insulating phase.[8,19] In addition, the MR exhibits opposite trends at low temperatures when the current is applied along the *a* or *b* crystallographic axis.[19] In contrast, in the vertical geometry, both bilayer and monolayer exhibit similar behaviors characterized by a smooth increase in the resistance upon cooling down followed by a more pronounced enhancement at low temperatures (below T*), following the same trend when the current is applied along the *a* or *b* axis (see **Supplementary Section 3.3**). This supports sensing

the out-of-plane component (*c* axis), as already reported for other vertical van der Waals heterostructures.[26–30]

Next, we consider the field dependence of the MR at 10 K (first panel in **Figure 2.e-f**). In the monolayer case (first panel in **Figure 2.e**), we observe that MR stays constant and equal to zero, within the experimental error, when the field is applied along the *b* axis, in agreement with the alignment of the spins along this easy axis. When the field is oriented along *a*, the MR stays almost null for fields below ~ 0.6 T, increasing up to a 4 % for fields above $B_{sat,\ a\ axis}$ ~ 1.0 T. Finally, a similar trend is observed when the field is applied along the *c* axis, exhibiting a positive increase in the MR from fields above ~ 0.7 T up to 2.5% for fields higher than $B_{sat,\ c\ axis}$ ~ 2.0 T. As we will see later on, these saturation fields are the fields required at 10 K to reorient the spins in the monolayer from the *b* direction to the *a* and *c* directions.

In the bilayer case (first panel in **Figure 2.f**), we observe large and negative MR characterized by a progressive field evolution when the field is applied along the *a* or *c* axis followed by an upturn (at *ca.* 0.65 T and 1.5 T, respectively) until the MR saturates and shows no field evolution. On the contrary, along the *b* axis, an abrupt MR drop appears. These tendencies are in line with the magnetic response of bulk CrSBr (**Figure 1.d**), as well as with the MR of the monolayer. Notably, the saturation fields for the *a* and *c* axis are comparable for monolayer, bilayer and bulk ($B_{sat,\ a\ axis}$ ~ 1.0 T, $B_{sat,\ c\ axis}$ ~ 2.0 T). In contrast, the field along *b* required to switch the layers from the antiferromagnetic to the ferromagnetic state, is significantly reduced from the bulk to the bilayer (from $B_{sat,\ b\ axis}$ ~ 0.6 T to $B_{sat,\ b\ axis}$ ~ 0.2 T). In some bilayer devices, we observe certain hysteresis along the *b* axis (**Supplementary Section 3**). The width of the hysteresis varies slightly between devices (from 0 T to ~ 0.07 T) and can be attributed to a non-perfect alignment

between the magnetic field and the crystal axis, as further corroborated by rotation experiments discussed below.

We also note that, for the van der Waals heterostructures based on few-layers graphene, the intrinsic graphene magneto-resistance features can be observed, especially for fields applied along the *c* direction. In addition, in the monolayer case, we observe a narrow peak centered at zero field for the few-layers graphene-based van der Waals heterostructures, that is absent in the metallic-based heterostructures incorporating 2H-$NbSe_2$ or 2H-TaS_2 instead of graphene. This can be attributed to a spin-polarized current in the few-layers graphene due to proximity effect with the CrSBr, as reported by Ghiasi *et al*.[8] In this line, we do not observe neither a significant voltage-gate dependence since the intrinsic graphene gate-dependence is the most significant signal (**Supplementary Section 3.4**).

The overall trends discussed above can be better visualized by considering both the temperature and field dependence of the magneto-transport behavior of our vertical van der Waals heterostructures (**Figure 2.e-f**). We remark that the MR is zero at room temperature, developing a negative magnetoresistance in the range 150 K -240 K, *i.e.*, just above the T_c of the layers, which appears as wings that persist down to *ca.* 100 K. This trend is observed for all the field orientations and can be related with the appearance of short-range ferromagnetic correlations above T_c, which is non unexpected for low-dimensional magnetic materials, being also in agreement with recent muon spin resonance and magnetic susceptibility experiments on bulk CrSBr.[10] Interestingly, in the monolayer we observe that when the field is applied along *b* the MR is zero below T_c and does not change with temperature. This demonstrates that the spin is locked along the *b* axis from temperatures as high as T_c. In contrast, when the field is applied along *a* or *c* directions one observes positive MR above certain field threshold, which shows a temperature dependence

(**Figure 2.d**). These are the fields required to reorient the spins from *b* to *a* and *c*, respectively. Below T*, this field-induced reorientation is concomitant with an enhancement of MR, thus supporting the appearance of a phase in which the spins of the layer are fully oriented along these two directions, while they will be fluctuating at higher temperatures. In the bilayer case this enhancement appears in the three directions below T* and is sharper (*ca.* 35% compared to *ca.* 4% in the monolayer) since it is primarily dominated by the magnetization switching of the two layers and then by the spin reorientation within the individual layer. In this scenario what was previously named as hidden order can be seen as a cooperative freezing of the spins both within and between the layers, which will be perfectly aligned along the direction of the applied magnetic fields for values above 0.2 T (*b* axis), 1 T (a axis) and 2 T (c axis).

Finally, for illustrating the differences between monolayer and multilayer cases, we rotate the magnetic field along the *a*-*b* plane (**Figure 3** and **Supplementary Section 3.3)**. For the monolayer, two clear regions can be observed, with MR ~ 0 (blue) and MR > 0 (red). In line with the experiments described in **Figure 2**, these regions correspond to the spins being aligned along *b* (MR = 0) and *a* (MR > 0). A different scenario is offered in the multilayer case (**Figure 3.b-c**). Both bilayer and trilayer exhibit similar trends with two-clear regions of high/low absolute MR value that can be related to the relative spin orientation between the ferromagnetic layers (parallel/antiparallel). Upon rotation, the switching from the antiparallel to the parallel configuration occurs at slightly different magnetic fields, being it maximum/minimum when the field is aligned along the *a*/*b* axis, in agreement with the observations above. For fields below 0.2 T, there is a progressive evolution of the MR from the *a* to the *b* axis, whereas, for fields in between ~ 0.2 T and ~ 0.6 T, a sharp transition to the high MR state is observed at different rotation values,

exhibiting a hysteretic behavior that depends on the value of the applied external magnetic field. Above ~ 1.0 T, there is only a very weak dependence of MR upon rotation.

Overall, comparing the monolayer with the multi-layer case, the observed trends are in stark contrast to what occurs in other 2D magnets, as CrI_3, where there is a marked effect depending on the odd/even number of layers[28] and a clear structural difference between bulk and atomically-thin layers.[31] As well, at low-temperatures, the absolute MR value is much larger for the multilayer case. This can be understood within a conventional spin-valve picture, taking into account a two-channel current model: when both layers are aligned ferromagnetically, the resistance across the heterostructure is smaller than when the layers are antiferromagnetically coupled.[32] We should remark that the values of MR for the multilayer devices are larger than the value reported for bulk and atomically-thin layers measured in a horizontal configuration.[8,11,19]

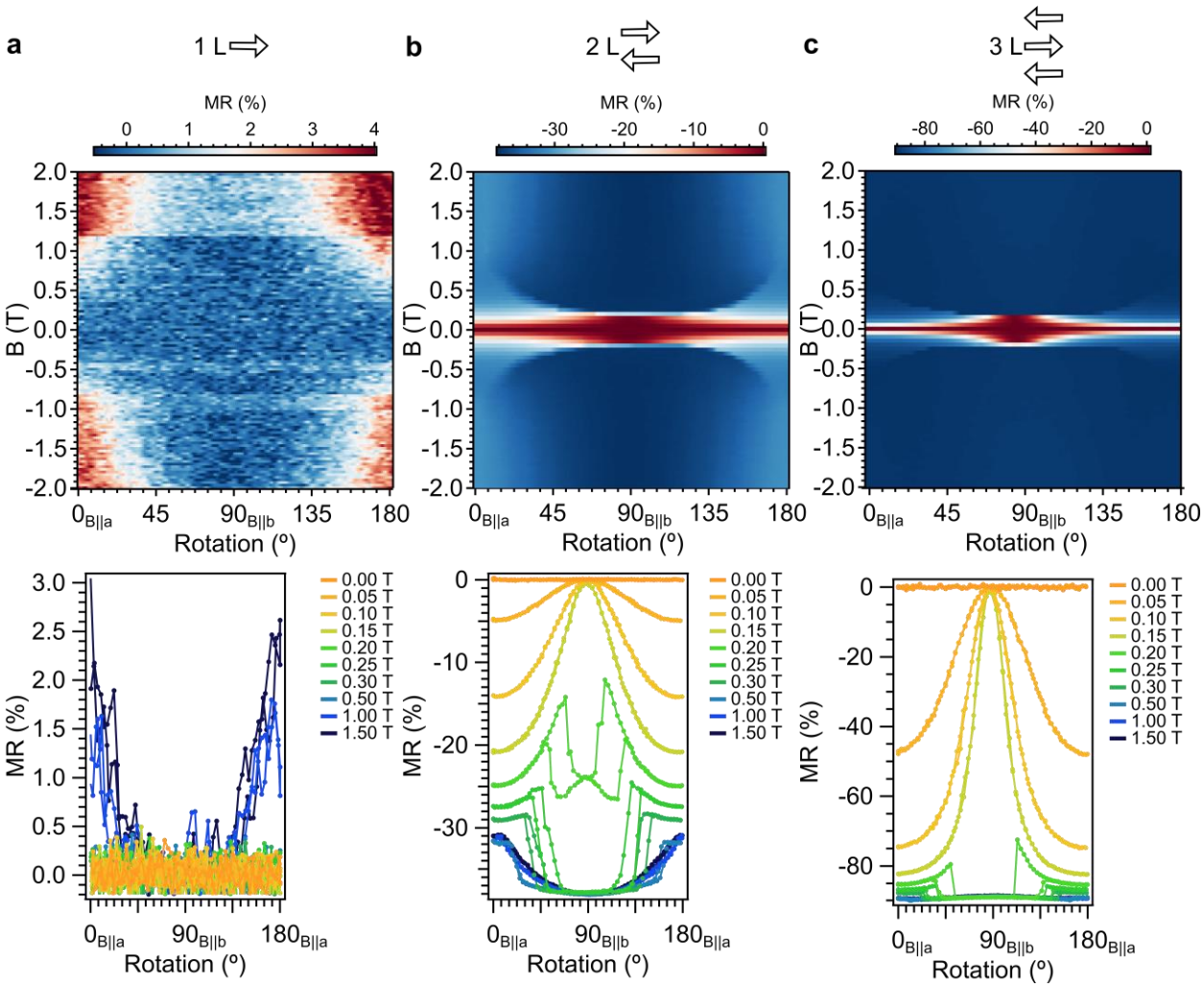

Figure 3.- Field orientation dependence of the magneto-transport properties of CrSBr van der Waals heterostructures in the *ab* plane. a) Monolayer CrSBr (device A.5 in the **Supplementary Information**). b) Bilayer CrSBr (device B.6 in the **Supplementary Information**). c) Trilayer CrSBr (device C.1 in the **Supplementary Information**).

In view of the previous experimental observations, we discuss here the influence of the magnetic field for inducing a spin-reorientation in this material. For this purpose, we have to take into account the magnetic anisotropy along the different axis. We perform DFT+U calculations for the three spin orientations including spin-orbit coupling (SOC) by using fully-relativistic pseudopotentials and computed the long-range magnetic dipole-dipole interactions.[12] (see **Supplementary Section 4** for further details). These calculations support that the most stable configuration is found for spins aligned along the *b* axis, followed by spins along *a* (anisotropy energy of 0.079 meV/Cr atom) and *c* (anisotropy energy of 0.215 meV/Cr atom). The total

anisotropy between the *a* and *b* directions is governed by the exchange term, while for the case between *b* and *c* the shape anisotropy consists on half of the exchange one, reflecting the typical behavior of shape anisotropy in 2D systems as it tends to align spins in plane. Based on these anisotropy energy differences, we estimate that the magnetic field needed for reorienting the spin from the easy magnetic axis (*b*) axis to the intermediate axis (*a*) is 0.45 T and 1.22 T to the hard-axis (*c*). These values are compatible with our experimental observations.

A second question of interest is that of rationalizing the interplay between the exchange network and the structural evolution of this compound with temperature. According to a Heisenberg exchange Hamiltonian, we define three exchange magnetic parameters J_1, J_2 and J_3 (**Figure 4.a-b**). J_1 is the first-neighbours exchange along *a* and it accounts for the interactions between Cr-Br-Cr (β) and Cr-S-Cr (α), while J_2 defines coupling between Cr atoms from different "sublayers" coupled along *c* (γ), and J_3 between Cr atoms mediated by S along the *b* axis (δ). By performing DFT+U+SOC calculations and constructing a derived tight-binding Hamiltonian expressed in the highly localized basis of Wannier functions for the most stable ferromagnetic (FM) configuration, we compute the exchange parameters as a function of the temperature. Given the DFT limitation of working at 0 K, we approximate the effect of temperature to the gradual variation of lattice parameters, extrapolating these data directly from experimental measurements and optimizing the atomic coordinates.[10] The three exchange parameters are ferromagnetic (in the range 2-4 meV; see **Supplementary Section 4**) and increase upon cooling down, tending to saturate at low temperatures (**Figure 4.c**). Interestingly, the exchange along the easy axis *b* (J_3) grows faster than the other two between 260 K and ca. 140 K, while below this temperature the increase in J_3 is lower and similar to that shown by J_1. In this region the thermal dependence of J_2 is almost zero. These trends are maintained when changing the values of Hubbard U in a typical

range to simulate the Coloumb interactions between the *d* electrons of Cr, i.e. from 3 eV to 5 eV (**Supplementary Section 4**). These also corroborate the close interplay between the magnetic lattice and the crystal structure. In fact, as the crystal cools down the magnetic ordering emerges and this has consequences on the *a*, *b*, and *c* lattice parameters, which follow different tendencies. While *a* tends to be enlarged due to an unconventional thermal expansion, both *b* and *c* get shorter following a conventional thermal compression in the range of temperatures from 240 K to 40 K.[10] This type of variation in the lattice parameters results in an increase of the three exchange parameters upon cooling down. Thus, it is tempting to assume that the unconventional expansion along *a* is triggered by magnetoelastic coupling, which try to maximize the ferromagnetic exchange coupling J_1 by increasing the angle Cr-S-Cr along *a* (α in **Figure 4.b**), while decreasing the angle Cr-S-Cr along *b* (δ in **Figure 4.b**). The variation in these two angles (from 94.9º to 95.1º for α and from 158.3º to 158.0º for δ upon cooling from 160K to 10K) enhance the corresponding ferromagnetic interactions according to the Goodenough-Kanamori rules. In fact, a linear dependence of J with the angle has been predicted (**Supplementary Section 4**). These results could be useful in the future to tune the magnetic ordering in these materials by applying uniaxial mechanical strain.

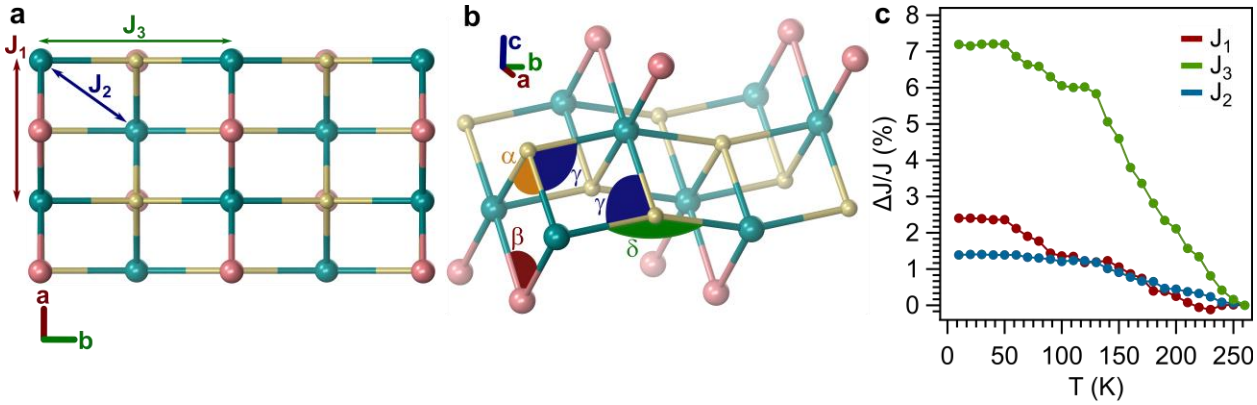

Figure 4.- Magnetic interactions in CrSBr. a) Top view of CrSBr monolayer pointing the J_1, J_2 and J_3 directions. b) Schematic representation of angles mediating the four different super-exchange paths. c) Change in J_1, J_2 and J_3 over temperature for a Hubbard U = 4 eV.

In this work, we have investigated the magneto-transport properties of CrSBr monolayers and bilayers incorporated into vertical van der Waals heterostructures. These results have unveiled some important questions related with the rich 2D physics exhibited by these low dimensional materials. In particular, our measurements in the monolayer limit have demonstrated the weak magnetic anisotropy of the magnetic layer, which has a ground state in which the spins are locked along the *b* axis from temperatures below $T_c \sim 150$ K (Ising-type spin anisotropy) but that can be reoriented towards the *a* and *c* axis upon application of modest magnetic fields along these directions (< 1 T and < 2 T, respectively). Interestingly, below a given temperature (30-40 K) the applied field seems to stabilize a cooperative state in which the spins are fully oriented (frozen) along the *a* and *c* directions, while above this temperature the reoriented spins are fluctuating due to the competition between magnetic and thermal energies. This scenario is reminiscent to that proposed by López-Paz[10] to explain the intriguing anomaly observed for the bulk at T*, but its origin is different. Here, the hidden order phase that should appear below T* is a field-induced state that depends on the magnetic anisotropy energy and, consequently, on the direction of the applied magnetic field. In the bilayer case this hidden-order is also a field-induced phase which is detected in the three crystallographic directions. Now, the influence of the field involves two processes: to switch the two antiferromagnetically-coupled ferromagnetic layers and to reorient the spins along the crystallographic axes. This makes the system of high interest not only as 2D magnetic model —different from the existing ones (as CrI_3 or Fe_3GeTe_2)— but also as spintronic component exhibiting spin-valve behavior with switching fields lower than those observed for the bulk and larger MR values.

Methods

Crystal growth: High quality crystals of CrSBr were grown by solid state techniques, as previously reported.[33] The crystal structure was verified by powder and single crystal X-ray diffraction as well as selected area electron diffraction in atomically-thin layers together with the elemental composition by energy-dispersive X-ray spectroscopy (see **Supplementary Section 1.1** for further details). Crystals of 2H-$NbSe_2$ and 2H-TaS_2 were grown by chemical vapor transport (CVT) using iodine as a transport agent, as already reported by some of us.[34]

Bulk magnetic measurements: Variable-temperature (2–300 K) direct current (d.c.) magnetic susceptibility measurements were carried out in an applied field of 1.0 kOe, and variable field magnetization measurements up to ±5 T, at 2.0 K. All the measurements were performed with a SQUID magnetometer (Quantum Design MPMS-XL-5).

X-ray diffraction: Single crystal X-ray diffraction measurements were performed as a function of temperature in the 10-75K range using a Microfocus Supernova diffractometer (Mo Kα radiation, λ = 0.71073 Å) equipped with a two dimensional ATLAS detector, and a Helijet He open flow cryosystem. A needle shape single crystal sample was cut from a very large block shape single crystal. Unit cell parameters were determined from 10K to 75K (5K step), while complete data collection for structural determination and analysis was performed at 10K and 75K. Analytical absorption corrections were applied. Initial structural models were based on those proposed by Beck,[13] and refined using full matrix least squares on F2 using OLEX.[35] More experimental and refinement details are provided in the supplementary information. The corresponding CIF files can be retrieved from Cambridge Structural Database (CSD) (deposition numbers: CCDC 2161029 & 2161030).

IR spectroscopy: All IR measurements were performed using a Nicolet 5700 FT-IR spectrometer equipped with a He closed-cycle cryostat. The sample was grinded, mixed with polyethylene powder, pressed into pellets, and glued to the cold-finger of the cryostat using silver-paste thermal adhesive. Measurements were carried out as a function of temperature from 300K to 10K in the 50-1000 cm-1 wavenumber range.

van der Waals heterostructure fabrication: Bulk crystals were mechanically exfoliated and placed on top of 285 nm SiO2/Si substrates using adhesive tape (80 μm-thick adhesive plastic film from Ultron Systems). The obtained flakes were examined by optical microscopy (NIKON Eclipse LV-100 optical microscope under normal incidence) as a fast tool for identifying the number of layers. The optical contrast was calculated as $C = (I_{flake} - I_{substrate})/(I_{flake} + I_{substrate})$,[36] with I_{flake} being the intensity of the 2D material and $I_{substrate}$ the intensity of the substrate (see **Supplementary Section 2** for further details). Atomic force microscopy images were taken with a Nano-Observer AFM from CSI Instruments. Once the desired atomically-thin layers were identified, the van der Waals heterostructure was fabricated by the deterministic assembly of the flakes using polycarbonate, as reported by Wang *et al.*,[37] using a micromanipulator. Finally, the stack of 2D materials (h-BN/few-layers graphene/CrSBr/few-layers graphene) was placed on top of pre-lithographed electrodes (5 nm Ti/50 nm Au on 285 nm SiO_2/Si from NOVA Electronic Materials, LCC). The whole process was performed under inert atmosphere conditions (argon glovebox).

TEM: Mechanical exfoliated flakes were transferred onto a silicon nitride (50 nm thick) membrane, as explained above. TEM images and diffraction patterns were acquired with a JEOL JEM-2100F with a field-emission gun operating at 200 kV. Simulated SAED patterns were generated with SingleCrystal software.

Electrical measurement setup: Electrical measurements were performed in a Quantum Design PPMS-9 cryostat with a 4-probe geometry, where a DC current was passed by the outer leads and the DC voltage drop was measured in the inner ones. DC voltages and DC currents were measured (MFLI from Zurich Instruments) using an external resistance of 1 MΩ, i.e., a resistance much larger than the sample. Temperature sweeps were performed at 1 $K \cdot min^{-1}$, field sweeps at 200 Oe/s and rotation sweeps at 3 °/s. For the resistance data, we consider different transport models (as energy-activated Arrhenius law or hopping mechanisms; see **Supplementary Section 3.5**), where different slope changes can be related with the magnetic ordering temperatures.

Computational details: We carried out first principles calculations based on spin-polarized density functional theory (DFT) in the plane wave formalism as implemented in the QuantumESPRESSO package.[38] The exchange-correlation energy is described by the generalized gradient approximation (GGA) using the Perdew–Burke–Ernzerhof (PBE)[39] functional and standard ultra-soft (USPP) solid-state pseudopotentials. The important role played by the strong correlations of the *d* electrons of the Cr^{3+} magnetic ions is simulated with a Hubbard-corrected DFT+U approach, choosing a standard on-site Hubbard U of 4 eV in the simplified version proposed by Dudarev *et al*.[40] We also evaluated U = 3 and 5 eV (see **Supplementary Section 4**). The electronic wave functions were expanded with well-converged kinetic energy cut-offs for the wave functions (charge density) of 60 (600). We used the experimental bulk lattice parameters determined by López-Paz *et al*.[10] between 10 and 270 K and optimized the atomic positions using the Broyden-Fletcher-Goldfarb-Shanno (BFGS) algorithm until the forces on each atom were smaller than $1 \cdot 10^{-5}$ Ry/au and the energy difference between two consecutive relaxation steps was less than $1 \cdot 10^{-7}$ Ry. To avoid unphysical interactions between images along the non-periodic direction, we add a vacuum of 18 Å in the *z* direction. The Brillouin zone was sampled by a fine Γ-centered 8 ×

8 × 1 k-point Monkhorst–Pack.[41] In order to determine exchange and magnetic anisotropy energy, we performed SOC calculations using fully-relativistic ultrasoft pseudopotentials with the spin oriented in each of the three spatial directions. For each one, we constructed a tight-binding model based on maximally localized Wannier functions[42] using the d orbitals of Cr, and p orbitals of S and Br as implemented in the Wannier90 package.[43] This allowed us to determine the isotropic Heisenberg parameters using the Green's function method as implemented in TB2J package[44] within a 20x20x1 supercell.

Corresponding Author

* samuel.manas@uv.es, eugenio.coronado@uv.es

Author Contributions

The work has been conceived by S.M.-V and E.C. C.B.-C and S.M.-V performed the growth, characterization and exfoliation of the crystals, the fabrication of the van der Waals heterostructures and fabrication of devices, their characterization and the magneto-transport measurements. A.M.R. and A.R. performed the theoretical calculations under the supervision of J.J.B. S.P. and K.A.K. performed the structural characterization and IR measurements at low temperatures. S.M.-V. and C.B.-C. wrote the first draft of the manuscript and E.C. supervised all the work and the preparation of the manuscript. All authors revised and contributed to the present manuscript.

Funding Sources

The authors acknowledge the financial support from the European Union (ERC AdG Mol-2D 788222), the Spanish MICINN (2D-HETEROS PID2020-117152RB-100, co-financed by FEDER,

and Excellence Unit “María de Maeztu” CEX2019-000919-M), the Generalitat Valenciana (PROMETEO Program and PO FEDER Program, IDIFEDER/2018/061, grant CDEIGENT/2019/022 and pre-doctoral fellowship GRISOLIAP/2021/038), the CNRS, the “Agence Nationale de la Recherche” (Project MolCoSM : Grant ANR-20-CE07-0028-03), and the Region Grand-Est. C.B.-C. thanks the Generalitat Valenciana for a Ph.D fellowship.

Notes

The authors declare no competing financial interest.

ACKNOWLEDGMENT

We thank J. M. Martínez-Agudo, G. Agustí and Á. López-Muñoz for their constant technical support and helpful discussions as well as S. Ferrer-Nicomedes regarding the optical contrast calibration of CrSBr atomically-thin layers and device fabrication.

REFERENCES

1. Gong, C. & Zhang, X. Two-dimensional magnetic crystals and emergent heterostructure devices. *Science* **363**, eaav4450 (2019).
2. Huang, B. *et al.* Layer-dependent ferromagnetism in a van der Waals crystal down to the monolayer limit. *Nature* **546**, 270–273 (2017).
3. Gong, C. *et al.* Discovery of intrinsic ferromagnetism in two-dimensional van der Waals crystals. *Nature* **546**, 265–269 (2017).
4. Šiškins, M. *et al.* Tunable strong coupling of mechanical resonance between spatially separated FePS$_3$ nanodrums. 1–22 (2021).
5. López-Cabrelles, J. *et al.* Isoreticular two-dimensional magnetic coordination polymers prepared through pre-synthetic ligand functionalization. *Nat. Chem.* **10**, 1001–1007 (2018).

6. López-Cabrelles, J. *et al.* Chemical Design and Magnetic Ordering in Thin Layers of 2D Metal–Organic Frameworks (MOFs). *J. Am. Chem. Soc.* **143**, 18502–18510 (2021).

7. Wu, Y. *et al.* Néel-type skyrmion in WTe2/Fe3GeTe2 van der Waals heterostructure. *Nat. Commun.* **11**, 3860 (2020).

8. Telford, E. J. *et al.* Hidden low-temperature magnetic order revealed through magnetotransport in monolayer CrSBr. (2021).

9. Wilson, N. P. *et al.* Interlayer electronic coupling on demand in a 2D magnetic semiconductor. *Nat. Mater.* (2021) doi:10.1038/s41563-021-01070-8.

10. López-Paz, S. A. *et al.* Dynamic Magnetic Crossover at the Origin of the Hidden-Order in van der Waals Antiferromagnet CrSBr. 1–12 (2022).

11. Telford, E. J. *et al.* Layered Antiferromagnetism Induces Large Negative Magnetoresistance in the van der Waals Semiconductor CrSBr. *Adv. Mater.* **32**, 2003240 (2020).

12. Yang, K., Wang, G., Liu, L., Lu, D. & Wu, H. Triaxial magnetic anisotropy in the two-dimensional ferromagnetic semiconductor CrSBr. *Phys. Rev. B* **104**, 144416 (2021).

13. Beck, J. Uber Chalkogenidhalogenide des Chroms Synthese, Kristallstruktur und Magnetismus von Chromsulfidbromid, CrSBr. *Zeitschrift fur Anorg. und Allg. Chemie* **585**, 157–167 (1990).

14. Göser, O., Paul, W. & Kahle, H. G. Magnetic properties of CrSBr. *J. Magn. Magn. Mater.* **92**, 129–136 (1990).

15. Wang, C. *et al.* A family of high-temperature ferromagnetic monolayers with locked spin-dichroism-mobility anisotropy: MnNX and CrCX (X = Cl, Br, I; C = S, Se, Te). *Sci. Bull.* **64**, 293–300 (2019).

16. Guo, Y., Zhang, Y., Yuan, S., Wang, B. & Wang, J. Chromium sulfide halide monolayers:

Intrinsic ferromagnetic semiconductors with large spin polarization and high carrier mobility. *Nanoscale* **10**, 18036–18042 (2018).

17. Wang, H., Qi, J. & Qian, X. Electrically tunable high Curie temperature two-dimensional ferromagnetism in van der Waals layered crystals. *Appl. Phys. Lett.* **117**, (2020).
18. Lee, K. *et al.* Magnetic Order and Symmetry in the 2D Semiconductor CrSBr. *Nano Lett.* **21**, 3511–3517 (2021).
19. Wu, F. *et al.* Quasi-1D Electronic Transport in a 2D Magnetic Semiconductor. *Adv. Mater.* 2109759 (2022) doi:10.1002/adma.202109759.
20. Ghiasi, T. S. *et al.* Electrical and thermal generation of spin currents by magnetic bilayer graphene. *Nat. Nanotechnol.* **16**, 788–794 (2021).
21. Kaverzin, A. A., Ghiasi, T. S., Dismukes, A. H., Roy, X. & van Wees, B. J. Towards fully two-dimensional spintronic devices. (2022).
22. Zhang, J. *et al.* Magnetoelastic coupling in the incommensurate antiferromagnetic phase of FeOCl. *Phys. Rev. B - Condens. Matter Mater. Phys.* **86**, 1–5 (2012).
23. Schönleber, A. *et al.* Phase transition, crystal structure, and magnetic order in VOCl. *Phys. Rev. B - Condens. Matter Mater. Phys.* **80**, 1–7 (2009).
24. Shaz, M. *et al.* Spin-Peierls transition in TiOCl. *Phys. Rev. B - Condens. Matter Mater. Phys.* **71**, 3–6 (2005).
25. Angelkort, J., Wölfel, A., Schönleber, A., Van Smaalen, S. & Kremer, R. K. Observation of strong magnetoelastic coupling in a first-order phase transition of CrOCl. *Phys. Rev. B - Condens. Matter Mater. Phys.* **80**, 1–6 (2009).
26. Boix-Constant, C., Mañas-Valero, S., Córdoba, R. & Coronado, E. Van Der Waals Heterostructures Based on Atomically-Thin Superconductors. *Adv. Electron. Mater.* **7**,

2000987 (2021).

27. Boix-Constant, C. *et al.* Out-of-Plane Transport of 1T-TaS 2 /Graphene-Based van der Waals Heterostructures. *ACS Nano* **15**, 11898–11907 (2021).

28. Klein, D. R. *et al.* Probing magnetism in 2D van der Waals crystalline insulators via electron tunneling. *Science* **360**, 1218–1222 (2018).

29. Klein, D. R. *et al.* Enhancement of interlayer exchange in an ultrathin two-dimensional magnet. *Nat. Phys.* **15**, 1255–1260 (2019).

30. Kim, H. H. *et al.* Evolution of interlayer and intralayer magnetism in three atomically thin chromium trihalides. *Proc. Natl. Acad. Sci. U. S. A.* **166**, 11131–11136 (2019).

31. Meseguer-Sánchez, J. *et al.* Coexistence of structural and magnetic phases in van der Waals magnet CrI3. *Nat. Commun.* **12**, 6265 (2021).

32. Ahn, E. C. 2D materials for spintronic devices. *npj 2D Mater. Appl.* **4**, 17 (2020).

33. Telford, E. J. *et al.* Layered Antiferromagnetism Induces Large Negative Magnetoresistance in the van der Waals Semiconductor CrSBr. *Adv. Mater.* **32**, (2020).

34. Pinilla-Cienfuegos, E. *et al.* Local Oxidation Nanolithography on Metallic Transition Metal Dichalcogenides Surfaces. *Appl. Sci.* **6**, 250 (2016).

35. Dolomanov, O. V., Bourhis, L. J., Gildea, R. J., Howard, J. A. K. & Puschmann, H. OLEX2 : a complete structure solution, refinement and analysis program. *J. Appl. Crystallogr.* **42**, 339–341 (2009).

36. Boix-Constant, C. *et al.* Strain Switching in van der Waals Heterostructures Triggered by a Spin-Crossover Metal–Organic Framework. *Adv. Mater.* **34**, 2110027 (2022).

37. Wang, L. *et al.* One-dimensional electrical contact to a two-dimensional material. *Science* **342**, 614–7 (2013).

38. Giannozzi, P. *et al.* QUANTUM ESPRESSO: a modular and open-source software project for quantum simulations of materials. *J. Phys. Condens. Matter* **21**, 395502 (2009).

39. Perdew, J. P., Burke, K. & Ernzerhof, M. Generalized gradient approximation made simple. *Phys. Rev. Lett.* **77**, 3865–3868 (1996).

40. Dudarev, S. L., Botton, G. A., Savrasov, S. Y., Humphreys, C. J. & Sutton, A. P. Electron-energy-loss spectra and the structural stability of nickel oxide: An LSDA+U study. *Phys. Rev. B* **57**, 1505–1509 (1998).

41. Monkhorst, H. J. & Pack, J. D. Special points for Brillouin-zone integrations. *Phys. Rev. B* **13**, 5188–5192 (1976).

42. Marzari, N. & Vanderbilt, D. Maximally localized generalized Wannier functions for composite energy bands. *Phys. Rev. B* **56**, 12847–12865 (1997).

43. Mostofi, A. A. *et al.* wannier90: A tool for obtaining maximally-localised Wannier functions. *Comput. Phys. Commun.* **178**, 685–699 (2008).

44. He, X., Helbig, N., Verstraete, M. J. & Bousquet, E. TB2J: A python package for computing magnetic interaction parameters. *Comput. Phys. Commun.* **264**, (2021).